

# Pixel-by-Pixel Spatiotemporal Progression of Focal Ischemia Derived Using Quantitative Perfusion and Diffusion Imaging

\*Qiang Shen, †Xiangjun Meng, †Marc Fisher, ‡Christopher H. Sotak, and  
\*‡#Timothy Q. Duong

\*Center for Comparative NeuroImaging, Departments of \*Psychiatry and †Neurology, #Programs in Neuroscience, Biomedical Engineering & Medical Physics, University of Massachusetts Medical Center; and ‡Department of Biomedical Engineering, Worcester Polytechnic Institute, Worcester, Massachusetts, U.S.A.

**Summary:** Pixel-by-pixel spatiotemporal progression of focal ischemia (permanent occlusion) in rats was investigated using quantitative perfusion and diffusion magnetic resonance imaging every 30 minutes for 3 hours. The normal left-hemisphere apparent diffusion coefficient (ADC) was  $0.76 \pm 0.03 \times 10^{-3} \text{ mm}^2/\text{s}$  and CBF was  $0.7 \pm 0.3 \text{ mL} \cdot \text{g}^{-1} \cdot \text{min}^{-1}$  (mean  $\pm$  SD,  $n = 5$ ). The ADC and CBF viability thresholds yielding the lesion volumes (LV) at 3 hours that best approximated the 2,3,5-triphenyltetrazolium chloride (TTC) infarct volumes ( $200 \pm 30 \text{ mm}^3$ ) at 24 hours were  $0.53 \pm 0.02 \times 10^{-3} \text{ mm}^2/\text{s}$  (30%  $\pm$  2% reduction) and  $0.30 \pm 0.09 \text{ mL} \cdot \text{g}^{-1} \cdot \text{min}^{-1}$  (57%  $\pm$  11% reduction), respectively. Temporal evolution of the ADC- and CBF-defined LV showed a significant “perfusion-diffusion mismatch” up to 2 hours ( $P < 0.05$ ,  $n = 11$ ), a potential therapeutic window. Based on the viability thresholds, three pixel clusters were identified on the CBF-ADC scatterplots: (1)

a “normal” cluster with normal CBF and ADC, (2) an “ischemic core” cluster with markedly reduced CBF and ADC, and (3) a “mismatch” cluster with reduced CBF but slightly reduced ADC. These clusters were color-coded and mapped onto the image and CBF-ADC spaces. Lesions grew peripheral and medial to the initial ADC abnormality. In contrast to the CBF distribution, the ADC distribution in the ischemic hemisphere was bimodal; the relatively time-invariant bimodal-ADC minima were  $0.57 \pm 0.02 \times 10^{-3} \text{ mm}^2/\text{s}$  (corresponding CBF  $0.35 \pm 0.04 \text{ mL} \cdot \text{g}^{-1} \cdot \text{min}^{-1}$ ), surprisingly similar to the TTC-derived thresholds. Together, these results illustrate an analysis approach to systemically track the pixel-by-pixel spatiotemporal progression of acute ischemic brain injury. **Key Words:** Penumbra—Oligemia—Perfusion—diffusion mismatch—Stroke—DWI—PWI.

Predicting tissue fate in ischemic injury is of critical importance in the treatment of ischemic brain injury. Data from experimental animal stroke models and stroke patients have shown that there is usually a gradual progression of potentially reversible cerebral ischemic injury toward infarction (Hossmann, 1995). A central core with severely compromised CBF is surrounded by a rim of moderately ischemic tissue with diminished CBF and impaired electrical activity but preserved cellular metabolism and viability, frequently referred to as the “ischemic penumbra” (Astrup et al., 1981). The transition from reversible to irreversible injury is complex and highly dependent on the duration and severity of ischemia, and as such different areas of the penumbra could

have variable outcomes. Reestablishing tissue perfusion and/or administering neuroprotective drugs in a timely fashion can salvage some ischemic tissues (Albers, 1999; NINDS, 1995). For example, clinical trials have shown the benefits of thrombolytic therapy within 3 hours after the onset of ischemia (Kidwell et al., 2000). To potentially help to expand the time window for thrombolytic therapy, it is critical to have the means to identify “tissue signature” and “clock window” to achieve the maximum benefit and to avoid devastating intraparenchymal hemorrhage (Albers, 1999). It is therefore important to establish noninvasive imaging techniques and analysis approach that can differentiate “salvageable” versus “nonsalvageable” tissues (Kaufmann, 1999; Schlaug et al., 1999).

Diffusion-weighted (DWI) and perfusion-weighted (PWI) magnetic resonance imaging (MRI) have been widely used to investigate cerebral ischemic injury in animal models and humans. Hyperintense regions on DWI correspond to tissues with a reduced apparent dif-

Received June 26, 2003; final version received September 19, 2003; accepted September 23, 2003.

Address correspondence and reprint requests to Dr. Duong, Center for Comparative NeuroImaging, University of Massachusetts Medical School, 55 Lake Avenue N, Worcester, MA 01655, U.S.A.; e-mail: timothy.duong@umassmed.edu

fusion coefficient (ADC) of water. Although the biophysical mechanism(s) underlying ADC reduction remains poorly understood and controversial (Duong et al., 1998, 2001; Moseley et al., 1990; Neil et al., 1996; Silva et al., 2002; van der Toorn et al., 1996; Wick et al., 1996; Zhong et al., 1993), the ADC decline has been correlated with energy failure and breakdown of membrane potential in animal models (Back, 1994; Hossmann, 1995; Kohno et al., 1995). Similarly, PWI yields a qualitative index of tissue perfusion. The most widely used PWI approach is based on dynamic imaging of an exogenous paramagnetic MRI contrast agent (Calamante et al., 1999). Hypointense regions on the PWI are indicative of reduced tissue perfusion. Quantitative perfusion and diffusion imaging could potentially yield a finer discrimination of tissue status based on their intrinsic diffusion and perfusion characteristics.

In humans, the "perfusion-diffusion mismatch" is presumed to approximate the ischemic penumbra. Although the strict definition of ischemic penumbra requires correlation with energy metabolism (Back, 1994; Hoehn-Berlage et al., 1995; Kohno et al., 1995) and such correlation is not feasible in humans, the ischemic penumbra and viability thresholds have been operationally defined based on DWI, PWI, and equivalent modalities. Schlaug et al. (1999), using DWI and PWI, reported the CBF in the ischemic core to be 12% of normal and the CBF in the penumbra to be 39% of normal. Kaufmann et al. (1999), using xenon computed tomography, reported a quantitative CBF value in the ischemic core of  $0.06 \text{ mL} \cdot \text{g}^{-1} \cdot \text{min}^{-1}$ , and in the ischemic penumbra between  $0.07$  and  $0.20 \text{ mL} \cdot \text{g}^{-1} \cdot \text{min}^{-1}$  in humans. Most studies to date involved region-of-interest (ROI) analysis. Although ROI analysis is helpful in simplifying a complex analysis problem, these ROIs contain tissues with different ADC and CBF characteristics, thereby inadvertently mixing the characteristics that one is trying to resolve. Pixel-by-pixel analysis combining quantitative diffusion and perfusion data without ROI prescription could offer a unique means to identify and predict ischemic tissue fate of individual pixels.

Although the "perfusion-diffusion mismatch" is widely observed in acute human stroke (Albers, 1999; Heiss and Graf, 1994; NINDS, 1995; Schlaug et al., 1999; Rohl et al., 2001), similar observations in animal stroke models have been limited and the temporal evolution of the perfusion-diffusion mismatch in animal models has yet to be systematically investigated. Animal models where focal ischemia can be reproducibly studied under controlled conditions would be important for identifying and predicting the severity of ischemic injury and for evaluating the efficacy of therapeutic intervention. In this study, we used *quantitative* perfusion and diffusion imaging to investigate the *temporal* and *spatial evolution* of focal ischemia after permanent intraluminal middle

cerebral artery occlusion (MCAO) in rats during the acute phase. We focused on quantitative perfusion and diffusion imaging of the acute phase because proton density (given by  $M_0$ ), T1 and T2 relaxation times are generally unaffected early after stroke onset and only begin to change with the advent of vasogenic edema (i.e., typically > 4 hours) (Helpert et al., 1993; Knight et al., 1994). The main goals were to establish and validate the absolute ADC and CBF viability thresholds below which tissues are destined to become infarcted, and to evaluate, *pixel-by-pixel*, the temporal and spatial evolution of ischemia using combined diffusion and perfusion analysis. These results were correlated with histology at 24 hours after ischemia.

## MATERIALS AND METHODS

### Animal preparations

Male Sprague-Dawley rats (300 to 350 g, Taconic Farms, NY, U.S.A.) were initially anesthetized intraperitoneally with choral hydrate (400 mg/kg, Sigma, St. Louis, MO, U.S.A.). The right femoral artery was catheterized for blood-gas sampling, continuous blood-pressure and heart-rate monitoring (BIOPAC, Santa Barbara, CA, U.S.A.). Permanent focal brain ischemia of the right hemisphere was induced using the intraluminal suture occlusion method (Li et al., 1999). Rectal temperature was maintained at  $36.5^\circ\text{C}$  to  $37.5^\circ\text{C}$  and respirations were recorded throughout the study. Anesthesia was switched to ~1% isoflurane once the animal was in the magnet and during imaging. Imaging was performed at 30, 60, 90, 120, and 180 minutes after occlusion, followed by TTC (2,3,5-triphenyltetrazolium chloride) staining for infarct volume at 24 hours (Li et al., 1999). Two groups of rats were studied. In group I ( $n = 5$ ), ADC and CBF thresholds were established. In group II ( $n = 6$ ), these thresholds were tested for reliability. All stroke rats survived 24 hours after ischemia.

### Magnetic resonance experiments

Magnetic resonance imaging was performed on a Bruker 4.7-T/40-cm magnet (Billerica, MA, U.S.A.) and a 20-G/cm gradient insert (12-cm inner diameter, 120- $\mu\text{s}$  rise time). The animal was placed into a stereotaxic headset and on the cradle, which had a built-in surface coil (2.3-cm inner diameter) for brain imaging and a neck coil for CBF labeling. Coil-to-coil electromagnetic interaction was actively decoupled.

The average apparent diffusion coefficient ( $\text{ADC}_{\text{av}}$ ) of water was obtained by averaging three ADC maps acquired separately with diffusion-sensitive gradients applied along the x, y, or z direction. Single-shot, spin-echo, echo-planar images (EPI) were acquired with a  $64 \times 64$  matrix,  $2.5 \times 1.9\text{-cm}^2$  field of view, six 1.5-mm slices, 2-second repetition time ( $90^\circ$  flip angle), 43-millisecond echo time,  $b$  values of 10 and  $1,504 \text{ s/mm}^2$ , 20-millisecond  $\Delta$ , 6.5-millisecond  $\delta$ , and 16 averages.

Quantitative CBF was measured using the continuous arterial spin-labeling technique (Duong et al., 2000; Sicard et al., 2003; Silva et al., 2000) with single-shot, gradient-echo EPI. MRI parameters were similar to the ADC measurement except that the echo time was 13 milliseconds. Labeling used a 1.78-second square radiofrequency pulse applied to the neck coil in the presence of a 1.0-G/cm gradient (Detre et al., 1992). Fifty pairs were acquired before and 50 pairs after the ADC measurement for signal averaging. Multislice CBF measurements

prevented the use of spin-echo EPI acquisition because of the relatively long spin-echo time. Although differences between spin-echo and gradient-echo EPI could cause pixel misalignment at the skull-brain interface and around the ear canals, this difference was minimized by using short gradient-echo time and careful shimming. Further, a conservative ROI avoiding the skull-brain interface was used for data analysis.

### Data analysis

For histologic analysis, brain slices were photographed and analyzed using the software BioScan OPTIMAS (Edmonds, WA, U.S.A.). Edema correction was applied (Tatlisumak et al., 1998). The MRI analysis used codes written in Matlab (MathWorks, Natick, MA, U.S.A.) and STIMULATE software (Strupp, 1996). Analysis was performed on conservative ROIs avoiding the brain-skull interface, which were carefully drawn based on CBF maps with reference to ADC maps and anatomical images to verify alignment. Statistical analysis was performed with the Student's paired *t*-test or repeated measure analysis of variance. A *P* value < 0.05 was considered to be statistically significant. Data are reported as mean  $\pm$  SD, and error bars on graphs are standard errors of the means (SEM).

**Calculation of ADC and CBF maps.** ADC<sub>av</sub> maps, in units of square millimeters per second, were calculated using the Stejskal-Tanner equation (Stejskal and Tanner, 1965). CBF maps, in units of milliliters per gram per minute, were calculated (Duong et al., 2000; Silva et al., 2000) using the water brain-blood partition coefficient ( $\lambda$ ) of 0.9 (Herscovitch and Raichle, 1985). Tissue T1 of 1.5 seconds and labeling efficiency ( $\alpha$ ) of 0.75 were measured using a method described elsewhere (Silva et al., 1995). Although consistent with many established techniques, the accuracy of this CBF technique could be subject to errors from the magnetization-transfer (Silva et al., 1995), transit-time (Calamante et al., 1996; Zhou et al., 2001), and water-exchange (Parkes and Tofts, 2002; Silva et al., 1997; Zhou et al., 2001) effects. The magnetization-transfer effect was not an issue with the actively decoupled two-coil system (Duong et al., 2000; Silva et al., 2000). Transit-time effect in small animals and water-exchange effect are small (Parkes and Tofts, 2002; Silva et al., 1997; Zhou et al., 2001) and unlikely to alter the conclusions of this study.

**ADC and CBF thresholds.** In group I, ADC and CBF thresholds were systematically lowered (via a Matlab program) until the CBF-defined and ADC-defined lesion volume (LV) at 3 hours numerically equal to the TTC infarct volume at 24 hours. This method set a fixed value below which the pixels within the ADC or CBF map were considered ischemic. The 3-hour time point was chosen because the ADC-derived LV of this stroke model was shown previously to stop evolving by this time (Reith et al., 1995). The same thresholds were then used to calculate the LV for all time points. In group II, the ADC-derived and CBF-derived LVs were determined using only the thresholds from group I, without using TTC information. The ADC-derived and CBF-derived LVs at 3 hours were independently correlated with TTC-derived infarct volume at 24 hours.

**Pixel-by-pixel analysis.** Pixel-by-pixel scatterplots of the CBF and ADC values were analyzed to evaluate the distribution of pixels over time. Only the center four slices were analyzed to minimize the misalignment between gradient-echo and spin-echo images around the ear canals. Four quadrants on the CBF-ADC scatterplots were derived using the TTC-derived ADC and CBF thresholds. The four zones were operationally defined as follows: (1) the "normal" cluster where both ADC and CBF were above the thresholds; (2) the "core" cluster where both ADC and CBF were below the thresholds; (3) the

"mismatch" cluster where the ADC was above the threshold but CBF was below the threshold; and (4) "zone 4" where ADC was below the threshold but CBF was above the threshold. Tissue volumes, means, and standard deviations of the ADC and CBF values of each cluster were evaluated at each time point. History of the pixels that eventually became infarcted was analyzed. The pixels from where the "core" (red) pixels came at the previous time points were colored blue in the CBF-ADC spaces. Projection profiles of the ADC and CBF distributions were also plotted at each time point.

## RESULTS

Blood gases, typically measured once during surgery and then 1 and 3 hours after occlusion, were not statistically different from each other and were grouped together. All blood gases (pH =  $7.36 \pm 0.02$ , Pco<sub>2</sub> =  $35 \pm 5$  mm Hg, Po<sub>2</sub> =  $83 \pm 8$  mm Hg, O<sub>2</sub> saturation =  $96 \pm 2\%$ ), heart rate ( $400 \pm 40$  bpm), mean arterial blood pressure ( $96 \pm 9$  mm Hg), and rectal temperature ( $37.0^\circ\text{C} \pm 0.5^\circ\text{C}$ ) were within normal physiologic ranges.

### Establishing and validating the ADC and CBF thresholds

The ADC and CBF thresholds were derived by setting the ADC-derived and CBF-derived LV at 3 hours after ischemia equal to the TTC-infarct volume at 24 hours (group I). The group-average ( $n = 5$ ) TTC-infarct volume was  $200 \pm 30$  mm<sup>3</sup>, normal CBF was  $0.7 \pm 0.3$  mL  $\cdot$  g<sup>-1</sup>  $\cdot$  min<sup>-1</sup>, CBF threshold was  $0.30 \pm 0.09$  ( $57 \pm 11\%$  reduction), normal ADC was  $0.76 \pm 0.03 \times 10^{-3}$  mm<sup>2</sup>/s, and ADC threshold was  $0.53 \pm 0.03 \times 10^{-3}$  mm<sup>2</sup>/s ( $30\% \pm 2\%$  reduction). Figures 1a and 1b show representative ADC and CBF maps as ischemia progressed from one animal. Hypointensity in the ADC and CBF maps indicates reduction in ADC and CBF values. Figure 1c shows the evolution of CBF and ADC lesion volumes from the same animal derived using the group-average viability thresholds. The CBF-defined LV was relatively constant across time. The ADC-defined LV started out small and grew with time. A significant perfusion-diffusion mismatch during the early acute phase was observed; as ischemia progressed, the ADC LV increased until it converged with the CBF LV at 3 hours.

These ADC and CBF thresholds were independently tested for reliability on a separate group of animals (group II,  $n = 6$ ) using only the ADC and CBF thresholds derived from group I. The group-average thresholds were also applied to group I. A repeated-measure analysis of variance of the temporal progression of MRI-derived LV curves showed no statistical differences between groups I and II ( $P > 0.05$ ); therefore, all subsequent analysis was applied to all 11 animals. There was a significant perfusion-diffusion mismatch between the CBF-derived and ADC-derived LVs during the acute phase. At 30, 60, 90, and 120 minutes, the ADC-derived LVs were  $68\% \pm 10\%$ ,  $81\% \pm 9\%$ ,  $87\% \pm 10\%$  and  $90\%$

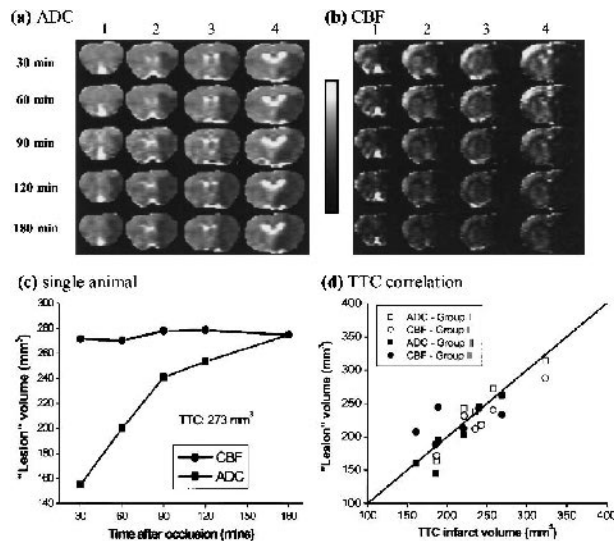


**FIG. 1.** Representative (a) ADC and (b) CBF maps from one animal. Four of six multislice ADC<sub>av</sub> and CBF maps are shown at 30, 60, 90, 120, and 180 minutes after ischemia. The grayscale bar indicates ADC ranges from 0 to 0.001 mm<sup>2</sup>/s and CBF ranges from -1 to 2 mL · g<sup>-1</sup> · min<sup>-1</sup>. (c) Temporal progression of ADC-defined and CBF-defined LV determined by using the group-average viability thresholds (57% and 30% reduction for CBF and ADC thresholds, respectively). The CBF LV remained constant over time. The ADC LV started out small and grew with time. TTC infarct volume of this animal was 273 mm<sup>3</sup>. (d) Correlation ADC-defined or CBF-defined LV versus TTC-infarct volumes. Data of group I and II were analyzed but separately. Correlation coefficient (*r*) and one-to-one correspondence (*y = x*) coefficient (*R*) were calculated. Filled squares, group I CBF (*r* = 0.98, *R* = 0.95); open squares, group II CBF (*r* = 0.95, *R* = 0.92); filled circles, group I ADC (*r* = 0.94, *R* = 0.99), open circles, group II ADC (*r* = 0.93, *R* = 0.99).

± 7% of the CBF-derived LVs, respectively (*P* < 0.05 up to 2 hours, *n* = 11). ADC-derived (230 ± 50 mm<sup>3</sup>) and CBF-defined (230 ± 40 mm<sup>3</sup>) LV at 3 hours was not statistically significant from the TTC infarct volumes at 24 hours (220 ± 40 mm<sup>3</sup>) (*P* > 0.05, *n* = 11). Excellent correlation and one-to-one correspondence analysis between the MRI-derived LV at 3 hours and TTC infarct volume at 24 hours further validated the ADC and CBF thresholds (Fig. 1d).

### Pixel-by-pixel analysis of ischemic progression

To further investigate the spatial dynamics of ischemia progression, pixel-by-pixel analysis was performed. Figure 2a shows the quantitative CBF-ADC scatterplots from one animal. The ADC-CBF distributions of the left hemisphere (LH) were markedly different from those of the right hemisphere (RH) at 30 and 180 minutes. In contrast to the single cluster in the normal LH, multiple clusters were observed in the ischemic RH and four zones were operationally defined based on the TTC-derived ADC and CBF thresholds. The three biologically relevant zones were: (1) the normal cluster with normal CBF and ADC; (2) the core cluster with marked reduced CBF and ADC; and (3) the “mismatch” cluster with re-

duced CBF but slightly reduced ADC. Essentially no pixels fell in zone 4 (reduced ADC but normal CBF) for this animal. The “mismatch” pixels were substantial at early time points and the majority of them migrated to the “core” zone by 180 minutes.

Pixels from the three zones were color-coded and mapped onto the image space (Fig. 2b). At 30 minutes after ischemia, the mismatch pixels (yellow) were substantial. As time evolved, the mismatch area decreased and, at 180 minutes, the majority (~80%) of the mismatch pixels had migrated into the core (orange); the remaining ~20% presumably arose from viable tissues with normal ADC but mild and sustained CBF reduction. The normal zone, on the other hand, was relatively time invariant. The “ischemic core” pixels (orange) grew as ischemia progressed and essentially all came from the mismatch zone. The detailed history of the core pixels at various time points is shown in Fig. 2c. In the ADC-CBF space, pixels that eventually became infarcted predominantly (90%) came from the mismatch zone, whereas only 10% of the pixels came from the normal zone. In the image spaces, ischemia developed predominantly medial and peripheral to the initial ischemic core.

Group-average results are shown in Fig. 3 (*n* = 11). The ADC and CBF of the LH were individually normalized to a zero mean for each animal. The ADC and CBF of the RH were computed relative to the LH at each time point. It should be noted that these group-average scatterplots contained variations of different tissue types and across subjects. Consistent with the single animal, the three biologically relevant zones in the RH were identified as follows: (1) the normal cluster with normal CBF (0.8 ± 0.3 mL · g<sup>-1</sup> · min<sup>-1</sup>) and ADC (0.75 ± 0.08 × 10<sup>-3</sup> mm<sup>2</sup>/s); (2) the core cluster with markedly reduced CBF (0.1 ± 0.1 mL · g<sup>-1</sup> · min<sup>-1</sup>) and ADC (0.43 ± 0.06 × 10<sup>-3</sup> mm<sup>2</sup>/s); and (3) the mismatch cluster with reduced CBF (0.18 ± 0.10 mL · g<sup>-1</sup> · min<sup>-1</sup>) but slightly reduced ADC (0.7 ± 0.1 × 10<sup>-3</sup> mm<sup>2</sup>/s). The mean ADC and CBF values of various clusters were not statistically different across time. Unlike the single animal data, some (20% of mismatch volume at 30 minutes) pixels remained in the mismatch zone at 180 minutes and there were some (17% of the core pixels) pixels in zone 4. The remaining mismatch pixels at 180 minutes arose from viable tissues with normal ADC but sustained (mild) CBF reduction, and/or from intersubject variations associated with the fixed thresholds. The former was visually confirmed by the ADC and CBF maps still showing a small persistent mismatch at 3 hours in some animals (data not shown). Pixels in zone 4 arose from intersubject variations associated with the use of fixed thresholds. Most of these pixels were identified as the ischemic core after overlaying them on the image spaces; zone 4 pixels were classified and plotted as “core.”

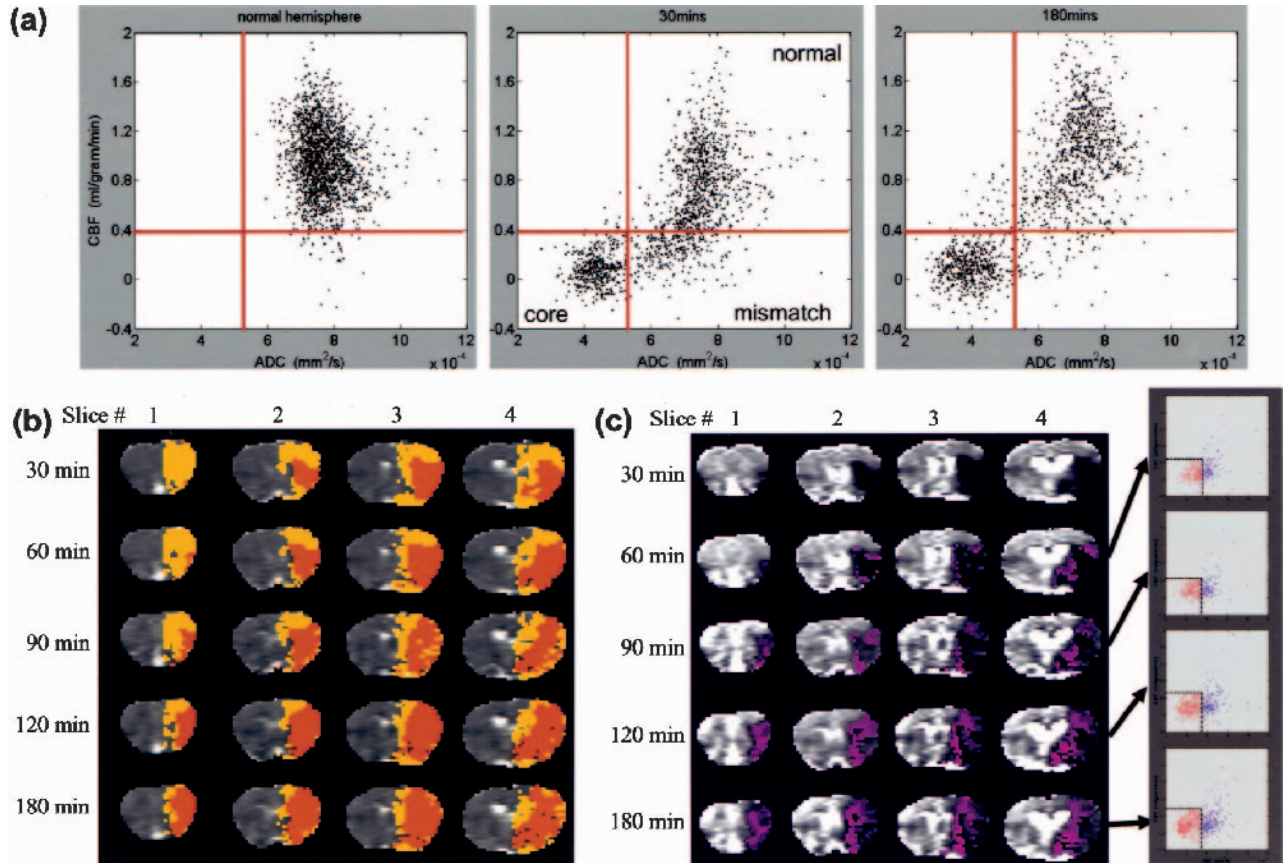


**FIG. 2.** (a) Pixel-by-pixel scatterplots of quantitative ADC and CBF maps of one animal in group II. Representative scatterplots were obtained from the left hemisphere (30 minutes), and the right hemisphere, separately, at 30 and 180 minutes after ischemia. The TTC-derived CBF and ADC group-average thresholds (solid red lines) are also superimposed on the scatterplots. (b) The spatial locations of the three clusters as ischemia progressed. Normal cluster was displayed in grayscale, core in orange, and mismatch in yellow. Zone 4 pixels constituted ~2% of total pixels in this animal and arose predominantly from the core zone based on their spatial location, were mapped as “core” pixels. (c) History of pixels that became infarcted. The blue pixels show from where the core (red) pixels came at the previous time points in the CBF-ADC space. These blue pixels were mapped on the image and ADC-CBF spaces.

Figure 4a shows the volume evolutions of the three clusters. As expected, the core volume increased as ischemia progressed and, at 180 minutes after ischemia, it reached 133% of the volume at 30 minutes. The mismatch volume, however, consistently decreased as ischemia progressed and, at 180 minutes after ischemia, it was 23% of the volume at 30 minutes. The normal volume decreased slightly as ischemia progressed and, at 180 minutes after ischemia, was 85% of the volume at 30 minutes.

Volume evolutions of the mismatch pixels at 30 minutes, as they evolved into different zones, are shown in Fig. 4b. By definition, the number of mismatch pixels at 30 minutes was maximum. As ischemia evolved, the mismatch volume decreased and, at 180 minutes after ischemia, the majority (80%) of the initial mismatch pixels migrated to the core.

**Projection-profile analysis**

Projection profiles of the ADC and CBF distributions were analyzed. In contrast to the LH, the RH ADC dis-

tribution was bimodal with a distinct separation (a minimum); such minima did not substantially change with time (Fig. 5a). The ADC bimodal minimum ( $ADC_{bimodal}$ ) was -24% reduction ( $0.57 \pm 0.02 \times 10^{-3} \text{ mm}^2/\text{s}$ ), and the corresponding CBF value ( $CBF_{bimodal}$ ) -56% reduction ( $0.35 \pm 0.04 \text{ mL} \cdot \text{g}^{-1} \cdot \text{min}^{-1}$ ), were surprisingly similar to the TTC-derived ADC (30% reduction,  $0.53 \pm 0.02 \times 10^{-3} \text{ mm}^2/\text{s}$ ) and CBF (-57% reduction,  $0.30 \pm 0.09 \text{ mL} \cdot \text{g}^{-1} \cdot \text{min}^{-1}$ ) thresholds, respectively. The small differences were likely due to errors in cross-modality comparison between histology and magnetic resonance data. The mean left-mode RH ADC ( $0.47 \pm 0.07 \times 10^{-3} \text{ mm}^2/\text{s}$ ) was markedly lower than the LH ADC and shifted to a lower ADC as ischemia progressed, whereas the mean right-mode RH ADC ( $0.71 \pm 0.07 \times 10^{-3} \text{ mm}^2/\text{s}$ ) was similar to the LH ADC and did not shift with time. The left-mode ADC volume increased and the right-mode ADC volume decreased as ischemia progressed. For the CBF distributions, the RH CBF was markedly lower than the LH CBF as expected. Unlike the RH ADC profiles, the RH CBF profiles were unimodal,

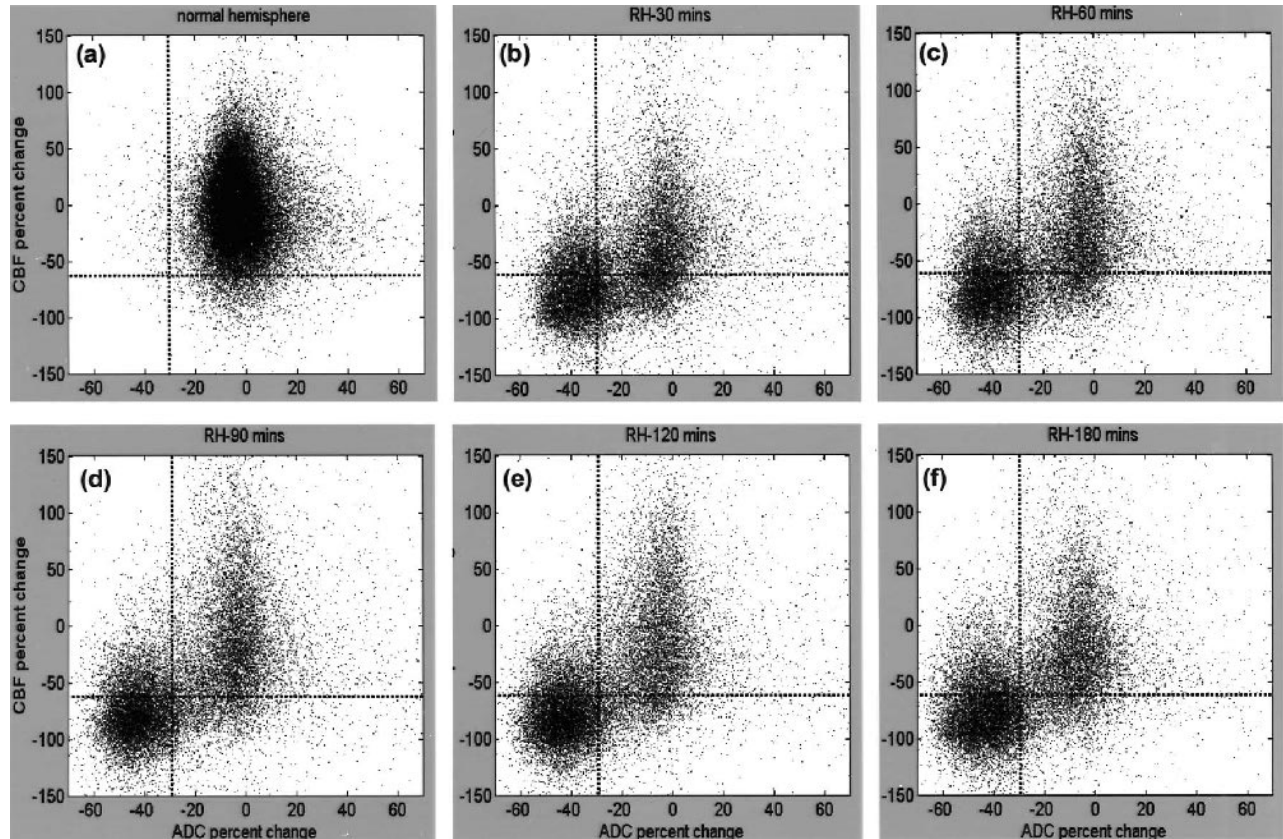


**FIG. 3.** Normalized pixel-by-pixel ADC-CBF scatterplots from all animals ( $n = 11$ ). Scatterplots were obtained from (a) the left hemisphere (~250,000 pixels for all five time points; all five time points were plotted together because LH ADC and LH CBF changes were not statistically different across time) and from the right hemisphere (~50,000 pixels at each time point) at (b) 30 minutes, (c) 60 minutes, (d) 90 minutes, (e) 120 minutes, and (f) 180 minutes after ischemia. Left-hemisphere CBF and ADC distribution means were  $0.8 \pm 0.3 \text{ mL} \cdot \text{g}^{-1} \cdot \text{min}^{-1}$  and  $0.75 \pm 0.08 \times 10^{-3} \text{ mm}^2/\text{s}$ , respectively. Superimposed as dotted lines on these plots are the TTC-derived CBF and ADC thresholds. Values reported in text were obtained with a limit of  $\pm 150\%$  of normal CBF and  $\pm 70\%$  of normal ADC as displayed; pixels outside of these limits were negligible (~2%) and arose from noise and/or pixels at the edge of the brain.

so different clusters could not be readily resolved based on CBF differences alone (Fig. 5b).

**DISCUSSION**

The major results of this study can be summarized as follows. (1) With the use of quantitative perfusion and

diffusion imaging, CBF and ADC viability thresholds in the permanent MCAO model in rats were established and independently tested for reliability. (2) Analysis of ischemia progression using these viability thresholds demonstrated that tissues at risk for infarction could be identified. (3) Pixel-by-pixel analysis of the ADC and CBF

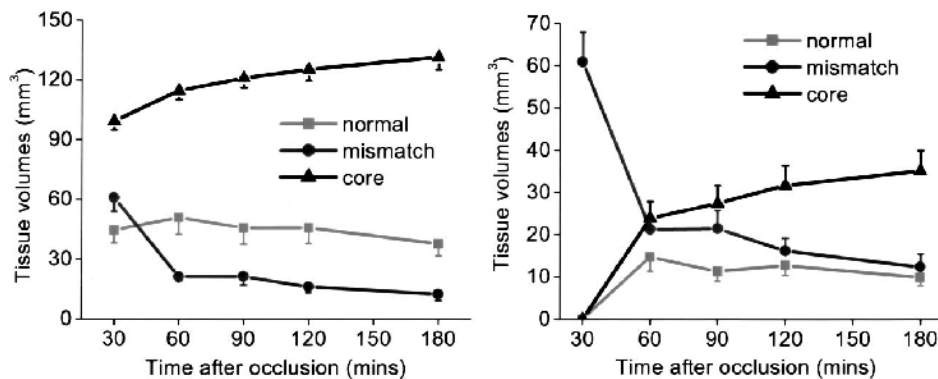


**FIG. 4.** (a) Temporal evolution of the tissue volumes of the four “clusters” derived from Fig. 3 ( $n = 11$ ): normal cluster, mismatch cluster, core cluster, and zone 4. Core and zone 4 were plotted together because they were the same tissue types based on their spatial location. (b) Temporal evolution of the tissue volumes of the mismatch cluster relative to 30 minutes after ischemia. At 30 minutes, all pixels belonged to the mismatch. As ischemia evolved, these pixels migrated to different clusters.

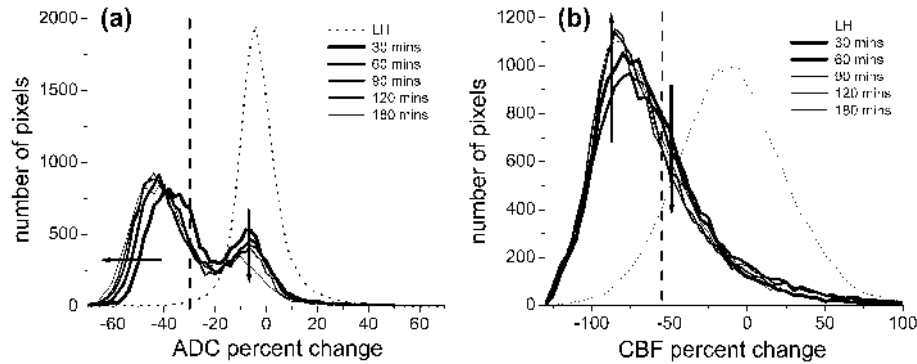


**FIG. 5.** Profiles of (a) ADC and (b) CBF from the scatterplots in Fig. 3 ( $n = 11$ ). Profiles were plotted for the entire left and the entire right hemisphere at each time point after ischemia. The ADC distribution was bimodal but the CBF was unimodal. The ADC bimodal minimum was at the  $-24\%$  mark ( $0.57 \pm 0.02 \times 10^{-3} \text{ mm}^2/\text{s}$ ) and the corresponding CBF value was at the  $-56\%$  mark ( $0.35 \pm 0.04 \text{ mL} \cdot \text{g}^{-1} \cdot \text{min}^{-1}$ ). Superimposed on these profiles are the vertical dotted lines indicating TTC-derived ADC ( $-30\%$ ) or CBF ( $-57\%$ ) thresholds. Arrows indicate the direction of changes with time.

tissue characteristics yielded three biologically relevant “clusters.” Tissue volumes, means, and standard deviations of the ADC and CBF distributions of each cluster could be quantified. Pixels of different clusters could be mapped onto the image and ADC-CBF spaces, thereby making it possible to evaluate the spatiotemporal ischemic progression on a pixel-by-pixel basis without prescribing ROIs. (4) Projection profiles showed bimodal ADC, but unimodal CBF, distributions. The  $\text{ADC}_{\text{bimodal}}$  and the corresponding  $\text{CBF}_{\text{bimodal}}$  were relatively time independent, similar to the TTC-derived thresholds. The  $\text{ADC}_{\text{bimodal}}$  and the corresponding  $\text{CBF}_{\text{bimodal}}$  could potentially be used to resolve different tissue clusters without histologic correlation.

Most of the analyses of stroke data were performed using the volumetric approach and involved the use of ROI analysis. Although ROI analysis is helpful in simplifying a complex analysis problem, these ROIs contain tissues with different ADC and CBF characteristics, thereby inadvertently mixing the characteristics that one is trying to resolve and oversimplifying the complex task of characterizing tissue viability. The complex temporal and spatial evolution of focal cerebral ischemia had prompted the use of various combinations of MRI parameters and more sophisticated analysis methods (Bezdek et al., 1993; Carano et al., 1998, 2000; Jacobs et al., 2000, 2001a,b; Jiang et al., 1997; Mitsias et al., 2002; Welch et al., 1995; Wu et al., 2001) for performing multiparametric segmentation on a pixel-by-pixel basis to predict stroke outcome. Jacobs et al. (2001a) used the ISODATA technique to analyze T1, T2, and DWI data in acute and chronic human stroke. Mitsias et al. (2002) extended this analysis to correlate the T1, T2, and DWI ISODATA results with PWI-delineated lesion volume in humans. Wu et al. (2001) used generalized linear model algorithms to analyze DWI and PWI data to predict tissue outcome in human stroke patients imaged within 12 hours of symptom onset. ISODATA analysis of T1, T2

and DWI had also been applied to animal stroke models (Jacobs et al., 2001b). Similarly, a multispectral K-mean/Fuzzy c-mean clustering approach with *a priori* assignment of the number of clusters in the data set has also been applied to investigate the ischemic penumbra using T2-weighted images, PWI, and DWI in a rat stroke model (Carano et al., 1998, 2000). In contrast to most previous studies in animal stroke models that used “qualitative” PWI and DWI, our study focused on quantitative perfusion and diffusion imaging of the acute phase ( $< 4$  hours) where proton density (given by  $M_0$ ), T1, and T2 relaxation times are generally unaffected but tissue perfusion and diffusion are dynamically evolving (Helpert, 1993; Knight et al., 1994). Our analysis, however, did not use the automated multiparametric segmentation approach because it was difficult to visually identify three biologically relevant clusters on the CBF-ADC scatterplots in the acute phase without *a priori* information. Therefore, as the first step, simple TTC thresholds was used to derive the three biologically relevant clusters. The disadvantage of this approach is that it is subjected to error of cross-modality comparison and these thresholds may or may not be valid across different stroke models. Despite some inherent drawbacks, the similarity between TTC-derived thresholds and the ADC bimodal minimum as well as the consistency of the spatiotemporal dynamics of the various clusters with expectation suggests that this approach yielded reasonably accurate information regarding tissue fates. The use of fixed viability CBF and ADC thresholds to delineate ischemic lesions across different time points had been suggested previously. Olah et al. (2001) established a ADC threshold by correlating the ADC-derived lesion volumes with lesion volumes defined by metabolic energy failure (ATP depletion stained by postmortem bioluminescent technique), and reported that an ADC-reduction threshold of 23% was a good estimate at all time points during the MCAO period as well as the early

phase of reperfusion. Similarly, Hoehn-Berlage et al. (1995) established a minimum CBF threshold ( $0.15$  to  $0.20 \text{ mL} \cdot \text{g}^{-1} \cdot \text{min}^{-1}$ ) by correlating CBF autoradiography with ATP depletion. Although our CBF and ADC thresholds are slightly higher than that reported previously, they are in principle applicable at all MCAO time points and during subsequent recirculation. The CBF threshold was further justified by the finding that the derived CBF lesion volume in the permanent occlusion group remained stable over the 3-hour imaging period (Meng et al., 2003), and by the natural separation in the ADC profile ( $\text{ADC}_{\text{bimodal}}$ ) which was consistent with the histology-derived thresholds. These observations together support the premise of using fixed TTC-derived thresholds to approximate different clusters of tissue fate. It should be noted that four clusters in our data set derived out of using two thresholds. More clusters may be present in our data if different number of thresholds were used (i.e., it is conceivable that another threshold exists for the oligemic zone). Multiple clusters (more than two) in stroke data have been suggested using ISODATA analysis where the cluster numbers were statistically determined (Nagesh et al., 1998).

#### Critical CBF values

Despite the limitations of various imaging methods and the imprecise definition of penumbra, the validity of the penumbra concept has been proven in several studies in which different treatments have been shown to reverse some ischemic tissues (Albers, 1999; Kidwell et al., 2000; NINDS, 1995). It has been postulated that there is a critical CBF threshold(s) below which tissues are destined to become infarcted. Critical CBF thresholds have been examined by correlation with DWI contrast, TTC staining, ATP metabolism, and other measurements (Busza et al., 1992; Hoehn-Berlage et al., 1995; Kohno et al., 1995; Machadom et al., 1995; Miyabe et al., 1996; Perez-Trepichio et al., 1995; Roussel et al., 1995). In a study in which blood flow of the carotid arteries in gerbils was gradually decreased, Busza et al. (1992), used hydrogen clearance technique, and found a critical CBF value of  $0.15$  to  $0.20 \text{ mL} \cdot \text{g}^{-1} \cdot \text{min}^{-1}$  below which DWI contrast was observed. Hoehn-Berlage et al. (1995), used CBF autoradiography, and reported a critical CBF threshold of  $0.18 \pm 0.10 \text{ mL} \cdot \text{g}^{-1} \cdot \text{min}^{-1}$  that corresponded to energy failure at 2 hours after ischemia in rats; the corresponding ADC was  $77\% \pm 3\%$  of normal. The CBF threshold that approximated lactate acidosis was shown to be  $0.31 \pm 0.11 \text{ mL} \cdot \text{g}^{-1} \cdot \text{min}^{-1}$  where ADC was  $90\% \pm 4\%$  of normal at 2 hours after ischemia in rats (Kohno et al., 1995). In this study, the CBF threshold of  $0.30 \pm 0.09 \text{ mL} \cdot \text{g}^{-1} \cdot \text{min}^{-1}$  and ADC threshold of  $0.53 \pm 0.03 \times 10^{-3} \text{ mm}^2/\text{s}$  best approximated the tissues that are destined to infarct in the permanent MCAO in rats. Although our data are in general agreement with the

above-mentioned studies, these comparisons suggest that different critical thresholds exist for different biologic events after ischemia and that these thresholds are dependent on animal models, anesthetics used, duration, and/or severity of ischemic injury, and the accuracy of cross-modality comparison. Although the wide CBF distribution arose largely from intrinsic tissue CBF heterogeneity, improved CBF accuracy could better define the CBF viability thresholds.

Hossmann (1995) has critically reviewed a series of biologic events at different critical CBF thresholds after ischemic injury. We interpreted our ADC and CBF values from different clusters in references to these biological events. The CBF of the ischemic core ( $0.1 \pm 0.1 \text{ mL} \cdot \text{g}^{-1} \cdot \text{min}^{-1}$ , this study) is consistent with the CBF values that lead to anoxic membrane depolarization and loss of cell-volume homeostasis; the corresponding ADC was  $0.43 \pm 0.06 \times 10^{-3} \text{ mm}^2/\text{s}$ . The CBF of the mismatch cluster ( $0.18 \pm 0.10 \text{ mL} \cdot \text{g}^{-1} \cdot \text{min}^{-1}$ , this study) is significantly above that of the ischemic core but corresponds to the *onset* of energy failure and loss of evoked potential activity; the corresponding ADC was  $0.7 \pm 0.1 \times 10^{-3} \text{ mm}^2/\text{s}$ . Our TTC-derived CBF threshold ( $0.30 \pm 0.09 \text{ mL} \cdot \text{g}^{-1} \cdot \text{min}^{-1}$ ) and the CBF associated with the ADC bimodal minimum ( $0.35 \pm 0.04 \text{ mL} \cdot \text{g}^{-1} \cdot \text{min}^{-1}$ ) are most consistent with the *onset* of reduced glucose metabolism and lactate acidosis but before energy failure; the corresponding ADC values were  $0.57 \pm 0.02 \times 10^{-3} \text{ mm}^2/\text{s}$  and  $0.53 \pm 0.03 \times 10^{-3} \text{ mm}^2/\text{s}$ , respectively.

#### ADC bimodal minimum

The  $\text{ADC}_{\text{bimodal}}$  and  $\text{CBF}_{\text{bimodal}}$  were relatively time independent and surprisingly similar to the TTC-derived thresholds. Further, preliminary analysis of the 60-minute transient occlusion data also showed similar ADC bimodal minimum before and after reperfusion. These observations could have important implications. One major implication is that an ADC bimodal separation exists (instead of a continuous distribution), suggesting that there is a critical (distinct) ADC value below which there are definitive changes in the tissue biophysical properties, likely to correlate with a major cellular event(s) in the cascades of ischemic injury. Both the  $\text{CBF}_{\text{bimodal}}$  and the TTC-derived threshold were similar to the CBF threshold for lactate acidosis and reduced glucose metabolism ( $0.31 \pm 0.11 \text{ mL} \cdot \text{g}^{-1} \cdot \text{min}^{-1}$ ) (Kohno et al., 1995) but significantly higher than the CBF threshold ( $0.18 \pm 0.10 \text{ mL} \cdot \text{g}^{-1} \cdot \text{min}^{-1}$ ) for energy failure and loss of cell-volume homeostasis (Hoehn-Berlage et al., 1995). However, the precise connection of these biological events to the biophysical mechanism(s) underlying ischemia-induced ADC reduction is unclear.

Another implication of the bimodal ADC minimum is that it can be used to guide the CBF analysis. In marked

contrast to the ADC distribution, the RH CBF distribution was continuous, and different clusters could not be resolved. By using the ADC bimodal minimum as a threshold, CBF values of the mismatch, normal, and core clusters were resolved.

Finally, another implication is that the ADC<sub>bimodal</sub> and CBF<sub>bimodal</sub> were surprisingly similar to the TTC-derived thresholds, which were determined independently. Our working hypothesis is that the ADC and CBF of the ADC bimodal minimum and the TTC-derived viability thresholds are the same. Future studies will focus on testing this hypothesis. If it were true, the ADC-bimodal minimum could be used to approximate the “viability threshold” without the need for histologic correlation and, as such, it could have potential clinical applications.

### CONCLUSION

Quantitative, instead of qualitative, perfusion and diffusion viability thresholds in a permanent MCAO model in rats were established and independently tested for reliability. Analysis of the ischemic progression showed a reproducible perfusion-diffusion mismatch and suggested the presence of a two-hour therapeutic window. Pixel-by-pixel analysis of CBF-ADC scatterplots offered a simple means to track the spatiotemporal progression of ischemic tissue fates. Such analysis yielded unique additional information that is not evident in analyzing DWI and PWI in the spatial domain. The approach demonstrated herein could be useful for monitoring the dynamic changes in cluster membership as a function of therapeutic intervention (e.g., reperfusion, or drug treatment), where such information may be more useful in predicting tissue outcome. The ADC bimodal minimum, derived without histological correlation, approximated the viability thresholds and, therefore, could have potential clinical applications.

**Acknowledgments:** The authors thank Drs. Craig Ferris and Jean King for continuing support and Erica Hennig for helpful discussions. This work was performed using the support from a Biomedical Engineering Grant from the Whitaker Foundation.

### REFERENCES

Albers GW (1999) Expanding the window for thrombolytic therapy in acute stroke: The potential role of acute MRI for patient selection. *Stroke* 30:2230–2237

Astrup J, Symon L, Siesjo BK (1981) Thresholds in cerebral ischemia: the ischemic penumbra. *Stroke* 12:723–725

Back T, Hoehn-Berlage M, Kohno K, Hossmann KA (1994) Diffusion nuclear magnetic resonance imaging in experimental stroke. Correlation with cerebral metabolites. *Stroke* 25:494–500

Bezdek JC, Hall LO, Clarke LP (1993) Review of MR image segmentation techniques using pattern recognition. *Med Phys* 20:1033–1048

Busza AL, Allen KL, King MD, van Bruggen N, Williams SR, Gadian DG (1992) Diffusion-weighted imaging studies of cerebral ische-

mia in gerbils: potential relevance to energy failure. *Stroke* 23:1602–1612

Calamante F, Thomas DL, Pell GS, Wiersma J, Turner R (1999) Measuring cerebral blood flow using magnetic resonance imaging techniques. *J Cereb Blood Flow Metab* 19:701–735

Calamante F, Williams SR, van Bruggen N, Kwong KK, Turner R (1996) A model for quantification of perfusion in pulsed labeling techniques. *NMR in Biomed* 9:79–83

Carano RA, Li F, Irie K, Helmer KG, Silva MD, Fisher M, Sotak CH (2000) Multispectral analysis of the temporal evolution of cerebral ischemia in the rat brain. *J Magn Reson Imaging* 12:842–858

Carano RAD, Takano K, Helmer KG, Tatlisumak T, Irie K, Petrucelli JD, Fisher M, Sotak CH (1998) Determination of focal ischemic lesion volume in the rat brain using multispectral analysis. *J Magn Reson Imaging* 8:1266–1278

Detre JA, Leigh JS, Williams DS, Koretsky AP (1992) Perfusion imaging. *Magn Reson Med* 23:37–45

Duong TQ, Ackerman JH, Ying HS, Neil JJ (1998) Evaluation of extra- and intracellular apparent diffusion in normal and globally ischemic rat brain via 19F NMR. *Magn Reson Med* 40:1–13

Duong TQ, Sehy JV, Yablonskiy DA, Snider BJ, Ackerman JH, Neil JJ (2001) Extracellular apparent diffusion in rat brain. *Magn Reson Med* 45:801–810

Duong TQ, Silva AC, Lee S-P, Kim S-G (2000) Functional MRI of calcium-dependent synaptic activity: cross correlation with CBF and BOLD measurements. *Magn Reson Med* 43:338–392

Heiss WD, Graf R (1994) The ischemic penumbra. *Curr Opin Neurol* 7:11–19

Helpert JA, Dereski MO, Knight RA, Ordidge RJ, Chopp M, Qing ZX (1993) Histopathological correlations of nuclear magnetic resonance imaging parameters in experimental cerebral ischemia. *Magn Reson Imaging* 11:241–246

Herscovitch P, Raichle ME (1985) What is the correct value for the brain-blood partition coefficient for water? *J Cereb Blood Flow Metab* 5:65–69

Hoehn-Berlage M, Noriss DG, Kohno K, Mies G, Leibfritz D, Hossmann K-A (1995) Evolution of regional changes in apparent diffusion coefficient during focal ischemia of rat brain: the relationship of quantitative diffusion NMR imaging to reduction in cerebral blood flow and metabolic disturbances. *J Cereb Blood Flow Metab* 15:1002–1011

Hossmann KA (1994) Viability thresholds and the penumbra of focal ischemia. *Ann Neurol* 36:557–565

Jacobs MA, Knight RA, Soltanian-Zadeh H, Zheng ZG, Goussev AV, Peck DJ, Windham JP, Chopp M (2000) Unsupervised segmentation of multiparameter MRI in experimental cerebral ischemia with comparison to T2, diffusion, and ADC MRI parameters and histopathological validation. *J Magn Reson Imaging* 11:425–437

Jacobs MA, Mitsias P, Soltanian-Zadeh H, Santhakumar S, Ghanei A, Hammond R, Peck DJ, Chopp M, Patel S (2001a) Multiparametric MRI tissue characterization in clinical stroke with correlation to clinical outcome: part 2. *Stroke* 32:950–957

Jacobs MA, Zhang ZG, Knight RA, Soltanian-Zadeh H, Goussev AV, Peck DJ, Chopp M (2001b) A model for multiparametric MRI tissue characterization in experimental cerebral ischemia with histological validation in rat: part 1. *Stroke* 32:943–949

Jiang Q, Chopp M, Zhang ZG, Knight RA, Jacobs MA, Windham JP, Peck DJ, Ewing JR, Welch KMA (1997) The temporal evolution of MRI tissue signatures after transient middle cerebral artery occlusion in rat. *J Neurol Sci* 145:15–23

Kaufmann AM, Firlik AD, Fukui MB, Weshler LR, Jungries CA, Yonas H (1999) Ischemic Core and Penumbra in Human Stroke. *Stroke* 30:93–99

Kidwell CS, Saver JL, Mattiello J, Starkman S, Vinuela F, Duckwiler G, Gobin P, Jahan R, Vespa P, Kalafut M, Alger JR (2000) Thrombolytic reversal of acute human cerebral ischemia injury shown by diffusion/perfusion magnetic resonance imaging. *Ann Neurol* 47:462–469

Knight RA, Dereski MO, Helpert JA, Ordidge RJ, Chopp M (1994) MRI assessment of evolving focal cerebral ischemia: comparison with histopathology in rats. *Stroke* 25:1252–1262

Kohno K, Hoehn-Berlage M, Mies G, Back T, Hossmann KA (1995) Relationship between diffusion-weighted MR images, cerebral

- blood flow, and energy state in experimental brain infarction. *Magn Reson Imag* 13:73–80
- Li F, Han SS, Tatlisumak T, Liu KF, Garcia JH, Sotak CH, Fisher M (1999) Reversal of acute apparent diffusion coefficient abnormalities and delayed neuronal death following transient focal cerebral ischemia in rats. *Ann Neurol* 46:333–342
- Mancuso A, Machadom BH, Karibe H, Rooney WD, Zarow GJ, Graham SH, Weiner MW, Weinstein PR (1995) Correlation of early reduction in the apparent diffusion coefficient of water with blood flow reduction during middle cerebral artery occlusion in rats. *Magn Reson Med* 34:368–377
- Meng X, Shen Q, Li F, Ratan M, Fisher M, Sotak CH, Duong TQ (2003) Quantitative assessment of temporal changes in the “perfusion/diffusion mismatch” following focal cerebral ischemia in the rat brain. *Proc Int Soc Magn Reson Med* 1:303
- Mitsias PD, Jacobs MA, Hammond R, Pasnoor M, Santhakumar S, Papamitsakis NIH, Soltanian-Zadeh H, Lu M, Chopp M, Patel SC (2002) Multiparametric MRI ISODATA ischemic lesion analysis correlation with the clinical neurological deficit and single-parameter MRI techniques. *Stroke* 2839–2844
- Miyabe M, Mori S, van Zijl PCM, Kirsch JR, Eleff SM, Koehler RC, Traystman RJ (1996) Correlation of the average water diffusion constant with cerebral blood flow and ischemic damage after transient middle cerebral artery occlusion in cats. *J Cereb Blood Flow Metab* 16:881–891
- Moseley ME, Cohen Y, Mintonovitch J, Chileuitt L, Chileuitt L, Shimizu H, Kucharczyk J, Wendland MF, Weinstein PR (1990) Early detection of regional cerebral ischemia in cats: comparison of diffusion- and T2-weighted MRI and spectroscopy. *Magn Reson Med* 14:330–346
- Nagesh V, Welch KM, Windham JP, Patel S, Levine SR, Hearshen D, Peck D, Robbins K, D’Olhaberriague L, Soltanian-Zadeh H, Boska MD (1998) Time course of ADCw changes in ischemic stroke: beyond the human eye. *Stroke* 29:1778–1782
- Neil JJ, Duong TQ, Ackerman JH (1996) Evaluation of intracellular diffusion in normal and globally-ischemic rat brain via 133Cs NMR. *Magn Reson Med* 35:329–335
- NINDS (1995) Tissue plasminogen activator for acute ischemic stroke. The National Institute of Neurological Disorder, and Stroke rt-PA Stroke Study Group. *N Engl J Med* 333:1581–1587
- Olah L, Wecker S, Hoehn M (2001) Relation of apparent diffusion coefficient changes and metabolic disturbance after 1 hour of focal cerebral ischemia and at different reperfusion phases in rats. *J Cereb Blood Flow Metab* 21:430–439
- Parkes LM, Tofts PS (2002) Improved accuracy of human cerebral blood perfusion measurements using arterial spin labeling: Accounting for capillary water permeability. *Magn Reson Med* 48:27–41
- Perez-Trepichio AD, Xue M, Ng TG, Majors AW, Furlan AJ, Awad IA, Jones SC (1995) Sensitivity of magnetic resonance diffusion-weighted imaging and regional relationship between the apparent diffusion coefficient and cerebral blood flow in rat focal cerebral ischemia. *Stroke* 26:667–675
- Reith W, Hasegawa Y, Latour LL, Dardzinski BJ, Sotak CH, Fisher M (1995) Multislice diffusion mapping for 3-D evolution of cerebral ischemia in a stroke model. *Neurology* 45:172–177
- Rohl L, Ostergaard L, Simonsen CZ, Vestergaard-Poulsen P, Andersen G, Sakoh M, Le Bihan D, Gyldensted C (2001) Viability thresholds of ischemic penumbra of hyperacute stroke defined by perfusion-weighted MRI and apparent diffusion coefficient. *Stroke* 32:1140–1146
- Roussel SA, van Bruggen N, King MD, Gadian DG (1995) Identification of collaterally perfused areas following focal cerebral ischemia in the rat by comparison of gradient echo and diffusion-weighted MRI. *J Cereb Blood Flow Metab* 15:578–586
- Schlaug G, Benfield A, Baird AE, Siewert B, Lovblad KO, Parker RA, Edelman RR, Warach S (1999) The ischemic penumbra: operationally defined by diffusion and perfusion MRI. *Neurology* 53:1528–1537
- Sicard K, Shen Q, Brevard M, Sullivan R, Ferris CF, King JA, Duong TQ (2003) Regional cerebral blood flow and BOLD response in conscious and anesthetized rats under basal and hypercapnic conditions: implications for fMRI studies. *J Cereb Blood Flow Metab* 23:472–481
- Silva AC, Williams D, Koretsky AP (1997) Evidence for the exchange of arterial spin-labeled water with tissue water in rat brain from diffusion-sensitized measurements of perfusion. *Magn Reson Med* 38:232–237
- Silva AC, Lee S-P, Iadecola C, Kim SG (2000) Early temporal characteristics of CBF and deoxyhemoglobin changes during somatosensory stimulation. *J Cereb Blood Flow Metab* 20:201–206
- Silva AC, Zhang W, Williams DS, Koretsky AP (1995) Multi-slice MRI of rat brain perfusion during amphetamine stimulation using arterial spin labeling. *Magn Reson Med* 33:209–214
- Silva MD, Omae T, Helmer KG, Li F, Fisher M, Sotak CH (2002) Separating changes in the intra- and extracellular water apparent diffusion coefficient following focal cerebral ischemia in the rat brain. *Magn Reson Med* 48:826–837
- Stejskal EO, Tanner JE (1965) Spin diffusion measurements: Spin echoes in the presence of a time-dependent field gradient. *J Chem Physics* 42:288–292
- Strupp JP (1996) Stimulate: a GUI based fMRI analysis software package. *Neuroimage* 3:S607
- Tatlisumak T, Carano RA, Takano K, Ogenorth TJ, Sotak CH, Fisher M (1998) A novel endothelin antagonist, A-127722, attenuates ischemic lesion size in rats with temporal middle cerebral artery occlusion: a diffusion and perfusion MRI study. *Stroke* 29:850–857
- van der Toorn A, Dijkhuizen RM, Tulleken CAF, Nicolay K (1996) Diffusion of metabolites in normal and ischemic rat brain measured by localized IH. *Magn Reson Med* 36:914–922
- Welch KM, Windham J, Knight RA, Nagesh V, Hugg JW, Jacobs M, Peck D, Booker P, Dereski MO, Levine SR (1995) A model to predict the histopathology of human stroke using diffusion and T2-weighted magnetic resonance imaging. *Stroke* 26:1983–1989
- Wick M, Nagatomo Y, Prielmeier F, Frahm J (1995) Alteration of intracellular metabolite diffusion in rat brain *in vivo* during ischemia and reperfusion. *Stroke* 26:1930–1933
- Wu O, Koroshetz WJ, Ostergard L, Buonanno FS, Copen W, Gonzales G, Rordorf G, Rosen BR, Schwamm LH, Weisskoff RM, Sorensen AG (2001) Predicting tissue outcome in acute human cerebral ischemia using combined diffusion- and perfusion-weighted MR imaging. *Stroke* 32:933–942
- Zhong J, Petroff AC, Prichard JW, Gore JC (1993) Changes in water diffusion and relaxation properties of rat cerebrum during status epilepticus. *Magn Reson Med* 30:241–246
- Zhou J, Wilson DA, Ulatowski JA, Traystman RJ, van Zijl PC (2001) Two-compartment exchange model for perfusion quantification using arterial spin tagging. *J Cereb Blood Flow Metab* 21:440–455